Low-Loss Super-Wide Band Antenna over Customized Substrate

Shaimaa A. Mohassieb[1], Eman G. Ouf[2], Khalid F. A. Hussein[2], May A. El-Hassan[2], Asmaa E. Farahat[2]

[1]Akhbar Elyom Academy, 6th October City, Egypt
[2]Electronics Research Institute (ERI),11843, Cairo, Egypt

Corresponding author: Asmaa E. Farahat (e-mail: asmaa@eri.sci.eg).

ABSTRACT In this work, a super wide band antenna is proposed to operate in the frequency band 2.3 − 23 GHz. The antenna has two planar arms with a modified diamond shape printed on the opposite faces of three-layer dielectric substrate. Each arm of the antenna is capacitively coupled to circular sector near its end to increase the impedance matching bandwidth. The dielectric substrate is customized to fit the shape of the antenna arms and the parasitic elements to reduce the dielectric loss. The substrate material is composed of three layers. The upper and lower layers are Rogers RO3003TM of 0.13 mm thickness and the middle layer is made of paper of 2.3 dielectric constant and 2.7 mm thickness. The antenna is fed through a wide band impedance matching balun. The antenna design stages are performed through electromagnetic simulations concerned with the parametric study to get the optimum antenna dimensions to numerically investigate the role of the parasitic element to enhance the antenna performance. A prototype of the proposed antenna is fabricated to validate the simulation results. The experimental measurements come in good agreement with the simulation results and both of them show that the antenna operates efficiently over the frequency band 2.3 − 23 GHz with minimum radiation efficiency of 97% and maximum gain of 5.2 dBi. The antenna has bandwidth to dimension ratio (BDR) of 1360.

INDEX TERMS Printed antenna, SWB antenna, Wideband impedance matching, Low-loss antenna, Antenna Balun.

I. INTRODUCTION

Compact and low-profile antennas are vital in many applications such as wireless communication, high-performance aircraft, spacecraft, satellite, and missile applications [1-3]. The range of frequencies 3.1 − 10.6 GHz has been allocated for unlicensed ultra-wideband (UWB) by the Federal Communications Commission (FCC) technology [1]. The UWB antennas have ratio bandwidth (RBW) of 3.4:1 but, unfortunately, not suitable for long-range mobile communications due to their slow adaptation rate, lower transmitted power, and long signal acquisition time [1-2]. A super wideband (SWB) antenna might be a good candidate to meet the future generations of mobile communication system requirements and are able to overcome the shortage of the UWB antennas. Moreover, the SWB technology provides higher channel capacity and improved time accuracy when compared to the UWB technology [4-5]. The SWB operation does not have specific operating frequency range unlike the UWB. The antennas with a minimum bandwidth ratio of 10: 1 for impedance matching are considered as SWB antennas. Various applications with varying operational frequency bands can be covered with a single SWB antenna that is functional for both short-range and long-range communications [1-5]. The challenge faced by SWB antenna designers is to reduce the antenna size without reducing the bandwidth or disturbing the radiation pattern stability. In the following, some recently published research papers concerned with the design and investigation of SWB antennas of planar structure are presented.

The work of [3] presents a SWB antenna fed through a coplanar waveguide (CPW) and comprised of a modified bowtie-shaped patch and two asymmetrical ground planes printed on an FR4 substrate to achieve a frequency band of 3.03 − 17.39 GHz. In [6], A compact and high gain SWB antenna 5.7 − 40 GHz is introduced. The antenna has a basic circular patch with partial ground and a copper reflector to realize gain and bandwidth enhancement. The work of [7] presents a small bulb shaped planar SWB antenna operating over the frequency band 2.8− 40 GHz using frequency selective surface. A compact concentric structured monopole patch antenna emerged from a traditional circular monopole antenna for SWB microwave application in the range 1.2-47 GHz is proposed and investigated in [8]. In [9], a circular-hexagonal fractal antenna with circular metallic patch and a transmission line with partial ground plane are used for designing a SWB antenna to achieve a frequency band ranging from 2.18

GHz to 44.5 GHz. The work of [10] proposes a SWB monopole antenna consisting of an octagonal-ring shaped patch. Both the patch and feed line are shifted off the center line with a notch made in the ground plane to get the antenna operational over the frequency band 2.6-31 GHz. The SWB antenna proposed in [11] operates in the frequency band 1.4-18.8 GHz and quite efficient in covering most of the widespread wireless applications. Textile SWB antenna with conformal characteristics is analyzed and designed in [12]. A frequency band 2.8-44 GHz is achieved but is not capable to be used in communication. A compact SWB antenna 2.840 GHz with stable and improved radiation is introduced in [13] using super wideband frequency selective surface with efficiency of about 80% and bandwidth dimension ration (BDR) of 1904.

This paper introduces a SWB antenna design with matched impedance between 2.3 and 23 GHz. The antenna is constructed as a dipole with diamond shape arms with blended corners, capacitively coupled to circular sector elements for wide impedance matching. The substrate has customized size to fit the conducting metal surface of the antenna and composed of three layers to implement a gradient profile of the dielectric constant for improving the impedance matching bandwidth. A wide band feeding balun is employed to feed the proposed two balanced antenna using the unbalanced coaxial line.

The present paper is organized as follows. Section II introduces the design of the antenna. Section III presents the antenna fabrication and measurements of the return loss compared to simulation. Section IV describes the process of measuring the gain and radiation patterns, and provides comparison with the simulation results. Section V demonstrates the simulation and measured gain and radiation efficiency with the frequency. Section VI gives some comparisons between the performance of the antenna proposed in the present work and other SWB antennas presented in recently published work. Finally, Section VII summarizes the conclusions of the present work.

II. DESIGN OF THE PROPOSED ANTENNA

A new design for a SWB antenna is proposed in this work. The antenna is constructed as two diamond shape arms fed through a wideband balun. The radiating antenna and the balun used for feeding the antenna are explained in the following sections.

A. DESIGN OF THE RADIATING ARMS OF THE ANTENNA

The design of the proposed SWB antenna is shown in Fig. 1 and 2. The antenna is constructed as a dipole of two tapered modified-diamond shape arms with blended corners, capacitively coupled to two parasitic circular sectors through a narrow gap to increase the impedance matching bandwidth.

The angular extension of each arm in any two-arm antennas helps to increase the operational bandwidth. However, the limited length of the antenna arms limits both the lower and higher frequencies of the operational band. Therefore, placing the capacitively coupled elements of the appropriate shape and dimensions near the end of each arm has the effect of adapting the antenna impedance by effectively adding a reactive load to original antenna arms. Thus, the total impedance seen at the antenna feeding port can be adjusted by setting the dimensions of the reactively coupled loads so as to reduce the imaginary part of the impedance and to get the real part as close as possible to 50 Ω. The mission of the antenna designer, in this case, is to arrive at the appropriate shape, dimensions, and placement of the capacitively coupled elements to realize the required bandwidth for impedance matching. Definitely, the most critical of this design is the shape and dimensions of the coupling gap.

The geometry of the upper and lower surface of the proposed antenna is shown in Figure 1. The optimum design parameters are given in Table 1. The substrate is composed of three layers. The upper and lower layers are Rogers RO3003^{TM} with $\varepsilon_{r1} = 3$ and height $h_1 = 0.13$ mm. The middle layer is made of quality paper with $\varepsilon_{r2} = 2.3$ and height $h_2 = 2.7$ mm. The substrate is cut with the same size and shape of the metallic conducting surface of the antenna arms. One arm is printed on the upper surface of the substrate and the other arm is printed on the other side as shown in Figure 1. The antenna is fed through a coaxial feeder using a wideband impedance matching balun. The balun structure is explained in the next section.

The super wideband characteristics of the antenna and its high efficiency are attributed to: (i) the wide angle ψ of the tapered shape arm that increases the bandwidth. (ii) Increasing the bandwidth through smoothing of the sharp corners of the tapered diamond shape arms. (iii) The capacitive coupling of the arms of the antenna with circular sector shape parasitic elements improves the antenna matching and, hence, increases the bandwidth. (iv) Cutting the substrate material on the shape of the metallic surfaces instead of using conventional rectangular substrate to reduce the dielectric losses. (v) Constructing the substrate with multilayer dielectric with different dielectric constants with certain profile reduces the dielectric losses and, hence, increases the radiation efficiency. (vi) Feeding the antenna using wideband balun increases the input impedance matching bandwidth. This balun is constructed from two circular pads with radii D_L and D_U, lower and upper diameters, respectively. The lower pad is connected to the outer conductor of the coaxial line as shown in Figure 2 and the upper pad is connected to the inner conductor of the line as shown Figure 1a. The radii of the upper and lower pads and the distance between them, L_P, controls the operating band.

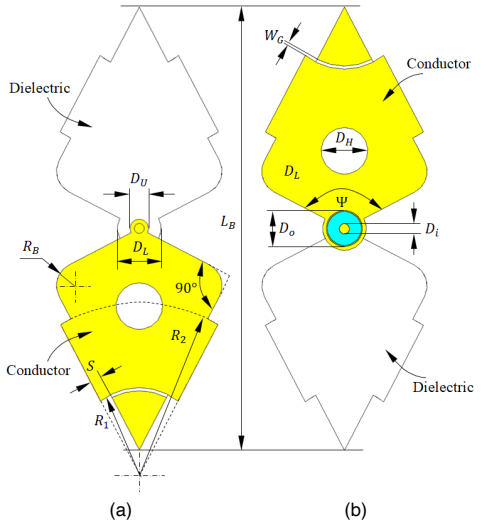

FIGURE 1: (a) Upper and (b) Lower surface of the proposed SWB antenna.

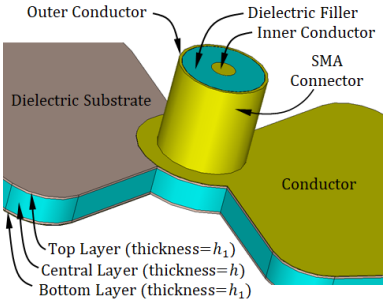

FIGURE 2: Substrate structure and the coaxial feeder connected to the antenna through the balun.

The final values of the dimensional parameters of the proposed antenna shown in Figure 1 are listed in Table 1. The optimum values of these parameters are obtained through extensive parametric study that is performed though electromagnetic simulations to investigate the effects of the various design parameters.

TABLE I. Optimum values of the dimensional parameters of the SWB antenna design presented in Figure 1.

Parameter	D_H	L_B	R_B	R_1	D_U	D_L	R_2
Value (mm)	4.8	57	3	8	2.6	6.4	19
Parameter	D_i	D_o	W_G	h	h_1	ψ	S
Value (mm)	1.3	4.45	0.4	2.6	0.13	125°	1.35

B. Smith Chart Plot for the Antenna Impedance

The variation of the antenna input impedance over the operational frequency band (2.3– 23 GHz) are plotted in a normalized smith chart in the plane of the reflection coefficient as shown in Figure 3. Five markers are placed on the graph to indicate the input impedance and the corresponding magnitude of the reflection coefficient at five different frequencies distributed over the entire frequency band. As the red curve approaches the center of the chart (zero-reflection coefficient), the antenna impedance is more matched. The markers at 3, 6, and 11 GHz show better impedance matching at these frequencies than the remaining frequencies of the operational band.

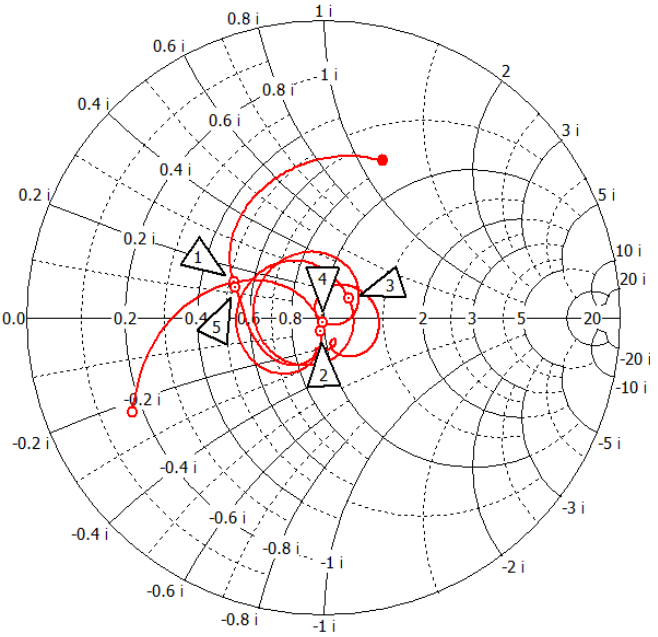

Marker	Frequency (GHz)	$\lvert S_{11}\rvert$ (dB)	$Z_{\text{in}}(\Omega)$	
			Real	Imaginary
1	2.3	−10	27.4	7.5
2	3	−27	51	−4.4
3	6	−20	61.2	8.2
4	11	−35	51.9	−1.2
5	23	−10	27.8	6.4

FIGURE 3: Impedance Smith chart showing the variation of the normalized input impedance (relative to 50 Ω) over the frequency band of operation with markers indicating the input impedance and the magnitude of the reflection coefficient at five different frequencies.

III. SIMULATION AND MEASUREMENT RESULTS

The proposed antenna is fabricated and experimental measurements are performed and compared to the simulation results in this section.

A. ANTENNA DESIGN THROUGH ELECTROMAGNETIC SIMULATION FOR PARAMETRIC STUDY

The radiating elements of the proposed antenna are the diamond shaped arms and the triangular parasitic elements. This sub-section is concerned with the presentation and discussion of some example of parametric studies to get the best values of the most important dimensional parameters including rhombic dipole length L_B, and the flare angle ψ_1.

The tapered modified diamond shape dipole length, L_B, strongly affect the operating band of the antenna. The reflection coefficient $|S_{11}|$ is calculated numerically for

different values of L_B in Figure 4, and found to have the best value (the wider operating bandwidth) at $L_B = 5.7$ cm.

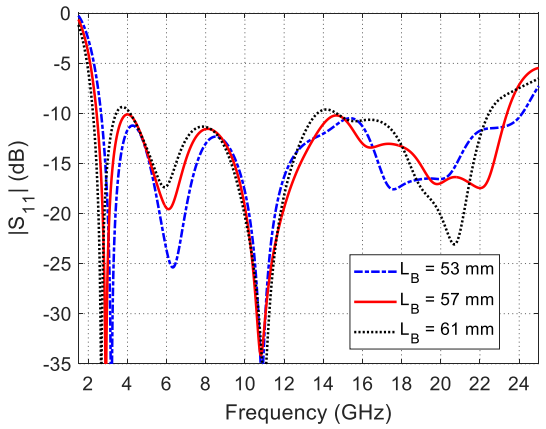

FIGURE 4: Calculated reflection coefficient $|S_{11}|$ with frequency for different values of the dipole arm length, L_B.

The flare angle ψ also can dramatically affect the operating band of the antenna. The optimum value for this angle is obtained when $\psi = 125°$. Figure 5 shows the simulated reflection coefficient for different values of the flare angle when $\psi = 115°, 125°, \text{and } 135°$.

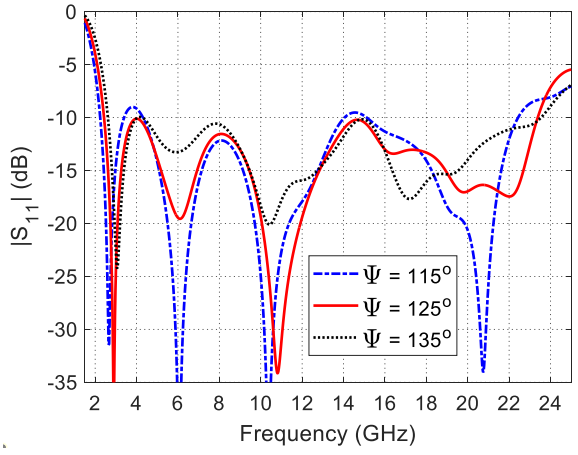

FIGURE 5: Calculated Reflection coefficient $|S_{11}|$ with frequency for different values of the flare angle ψ.

The effect of the distance between the upper and lower circular discs of the probe L_P, which is also the substrate height, h, on the reflection coefficient of the antenna is studied numerically using the CST simulator. The results are shown in Figure 6. The best value for L_P is found to 2.6 which results in the wider impedance matching over the required operating frequency band $(2.3 - 23$ GHz).

The two circular discs of the feeding balun affect the impedance matching bandwidth of the antenna. In Figure 7 and 8, the effect of the upper pad diameter D_U and lower pad diameter D_L of the feeding balun, respectively, on the frequency response of $|S_{11}|$ are plotted at different values. It is shown that the best value of D_U =1.9 mm $D_L = 6$ mm which results in perfect impedance matching over the frequency band $(2.3 - 23$ GHz).

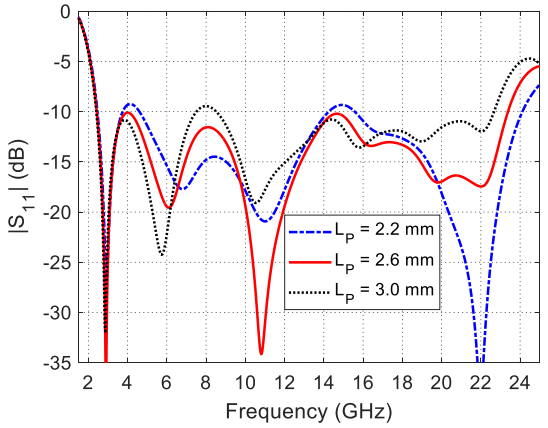

FIGURE 6: Calculated Reflection coefficient $|S_{11}|$ with frequency with varying the distance between the two balun discs, L_P.

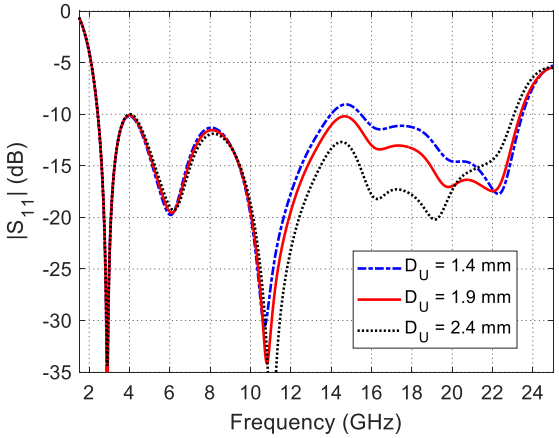

FIGURE 7: Calculated Reflection coefficient $|S_{11}|$ with frequency for different values of outer diameter of the upper circular pad of the balun, D_U.

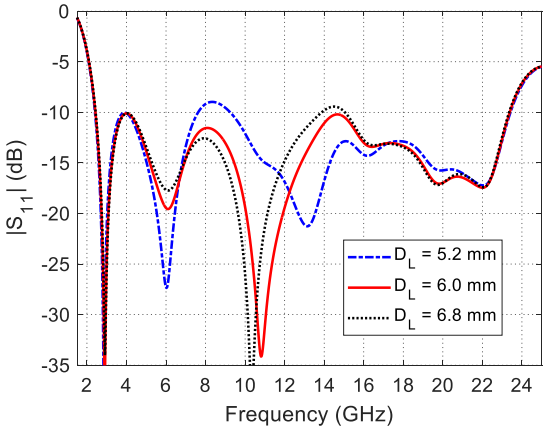

FIGURE 8: Calculated Reflection coefficient $|S_{11}|$ with frequency for different values of outer diameter of the lower circular pad of the balun, D_L.Calculated.

B. Effect of the Parasitic Elements at the Ends of the Antenna Arms

To present the role of the triangular parasitic elements at the end of each arm of the antenna, three alternative designs of the SWB two-arm antenna are discussed. The three antenna structures are illustrated in Figure 9. Ant.1 has neither the metallic parasitic element nor the triangular extension of the dielectric substrate. Ant.2 has the triangular substrate

extension without the metallic parasitic element. Ant.3 has the complete structure proposed in the present work. It should be noted that the three designs have the dimensions listed in Table 1. These can be considered as some of the design stages to arrive at the complete structure of the antenna proposed in the present work. As each parasitic element is separated from one of the antenna arms by a narrow gap, only the displacement current (or, equivalently, the electric field in the gap) can couple the power from the metallic arm to the metallic parasitic element (like a capacitor). Therefore, the parasitic element is considered as "capacitively" coupled to the corresponding arm. To explain the role of these triangular parasitic elements in improving the impedance matching and enhancement of its frequency band, the frequency responses of the reflection coefficient of the three antennas are presented in Figure 10. It is shown that removing the parasitic element and the underlying extension of the dielectric substrate results in the structure of Ant.1 whose impedance matching band has a lower frequency of 2.41 GHz and RBW of 9.5. Adding the triangular extension of the dielectric substrate results in the structure of Ant.2 whose lower frequency is 2.37 GHz and RBW is 9.7. The complete structure of the proposed antenna (Ant.3) with the triangular extension of the substrate and the metallic parasitic element has the best performance as the impedance matching bandwidth starts at 2.29 GHz and the RBW is 10.04. Moreover, the return loss of Ant.3 is much lower than those of Ant.1 and Ant.2 over a wide frequency range around the middle of the frequency band as shown in Figure 10.

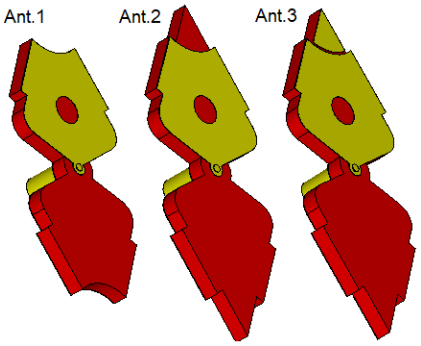

FIGURE 9: Three alternative designs of SWB two-arm antenna: Ant.1 has neither the metallic parasitic element nor the triangular extension of the dielectric substrate. Ant.2 has the triangular substrate extension without the metallic parasitic element. Ant.3 has the complete structure proposed in the present work.

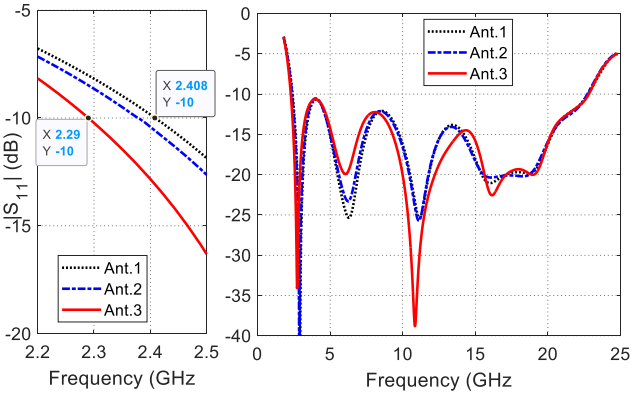

FIGURE 10: Effect of the parasitic elements at the ends of the antenna arms on the frequency response of the reflection coefficient. (a) Zoomed view at the lower frequency of the impedance matching band. (b) Variation of $|S_{11}|$ over the entire frequency band.

C. SURFACE CURRENT DISTRIBUTION AND RADIATION MECHANISM

The surface current distribution is calculated numerically at different frequencies. At the start of the impedance matching bandwidth at 3 GHz, the surface current distribution is shown in Figure 11a. It can be seen that the effective area that has the significant current magnitude is the area near the feeding on the diamond shape arm. This results in the radiation pattern shown in Figure 11b.

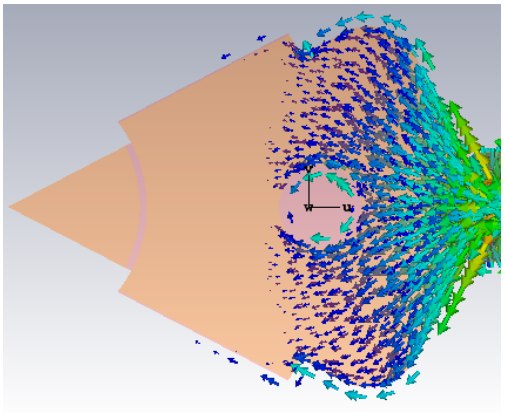

(a)

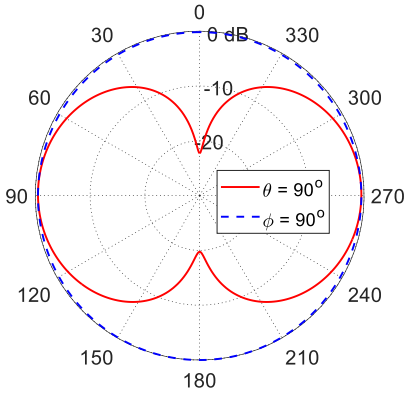

(b)

FIGURE 11: (a) Surface current distribution, (b) Radiation pattern, at 3 GHz.

In the middle of the operating band at 11 GHz, the surface current distribution is investigated in Figure 12a. As can be seen from the figure, a null is present at the arm center which indicates a second order mode. Also, a significant current is present on the triangular parasitic element. At this frequency, the main arm and the parasitic element contribute to the far-field radiation. The radiation from parasitic element has compensated the nulls in the radiation pattern resulting in the near isotropic pattern shown in Figure 12b.

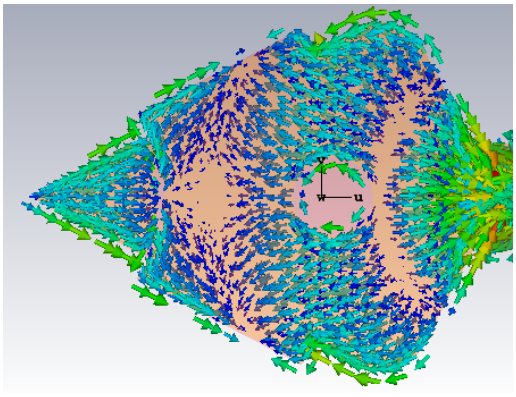

(a)

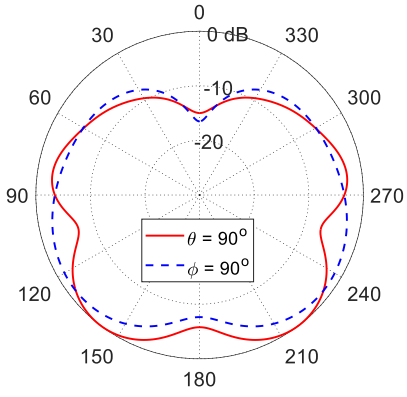

(b)

FIGURE 12: (a) Surface current distribution, (b) Radiation pattern, at 11 GHz.

At 22 GHz, the surface current has a higher order mode which can be seen from the distribution present in Figure 13a. The presence of higher order mode current results in a radiation pattern with nulls at 22 GHz. The radiation pattern is shown in Figure 13b.

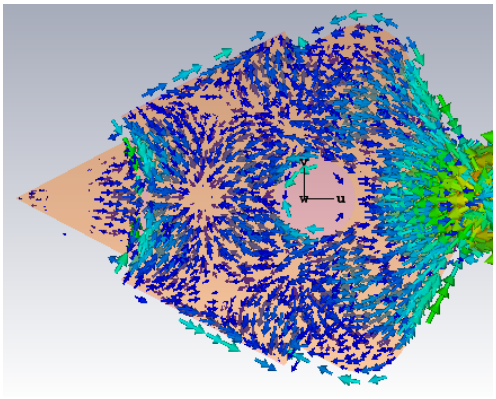

(a)

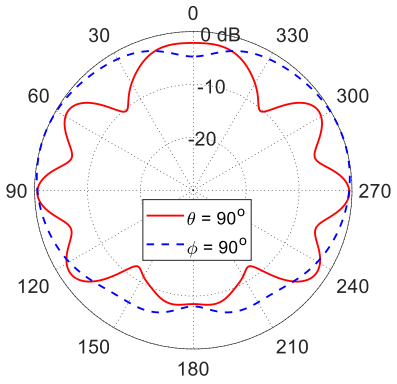

(b)

FIGURE 13: (a) Surface current distribution, (b) Radiation pattern, at 22 GHz.

D. FABRICATION AND MEASUREMENTS OF THE REFLECTION COEFFICIENT

After performing the electromagnetic simulations and obtaining the best values for the antenna design parameters given in table 1, a prototype is fabricated for the experimental verifications and measurements. The experimental results are compared to those obtained by the CST simulator regarding the reflection coefficient, radiation pattern, gain, and the radiation efficiency. The top and bottom view of the proposed antenna is shown in Figure 14a and 14b, respectively. An image of the fabricated prototype is presented in Figure 14c showing the SMA coaxial connector when welded at the antenna input. The inner conductor is welded with the upper circular disc of the balun and the outer conductor is soldered to the lower disc of the balun.

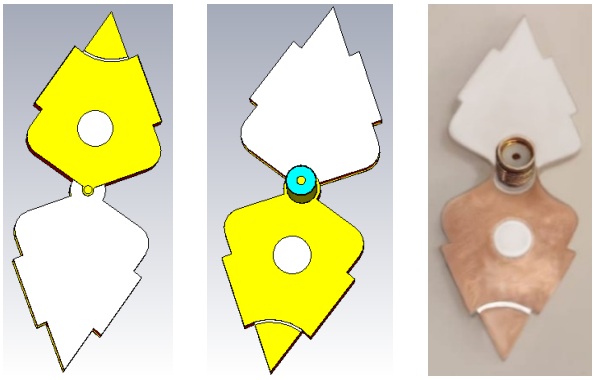

(a) (b) (c)

FIGURE 14: SWB antenna design (a) Top view, (b) Bottom view, (c) Fabricated prototype.

The vector network analyser (VNA) model Keysight N9918A is used to measure the reflection coefficient at the antenna input port. Firstly, the VNA is calibrated using the calibration kit Keysight 85521A. The antenna is then connected to the VNA using a semi-rigid coaxial cable to connect the SMA connector of the antenna to the VNA input port, as shown in Figure 15a. The magnitudes of the measured and simulated reflection coefficient S_{11} versus frequency are plotted in Figure 16 showing good agreement. As can be seen in Figure 16, the operating band below -10 dB extends from about 2.3 GHz to greater than 23 GHz for both the simulation and the measured return loss.

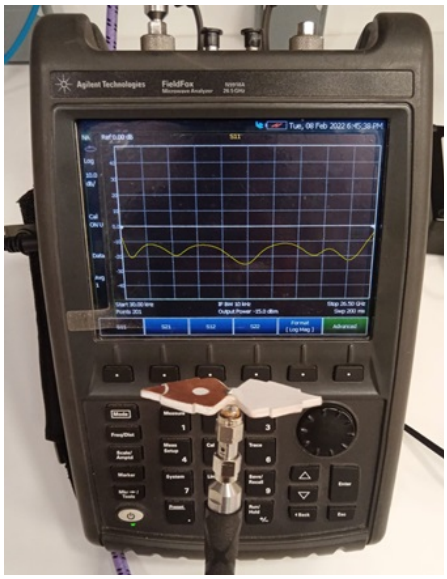

FIGURE 15: The connection of the fabricated antenna prototype to the VNA N9918A for measuring the reflection coefficient over the operating frequency band.

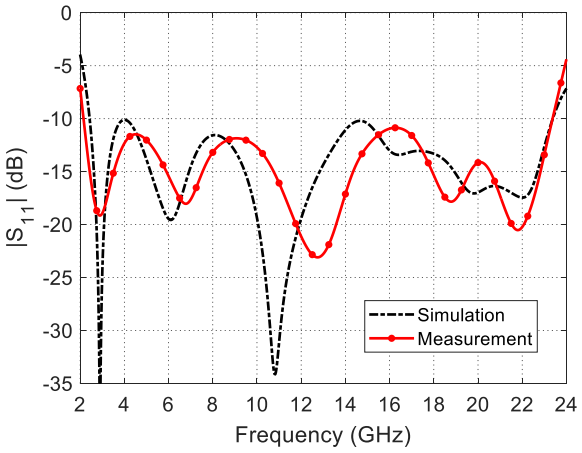

FIGURE 16: Measured and simulated reflection coefficient for the designed and fabricated SWB antenna.

E. RADIATION PATTERNS

In this section, the Far-field patterns of the proposed antenna are calculated and measured experimentally in the two principle planes $\phi = 0^{\circ}$ and $\theta = 90^{\circ}$. In Figures 17 and 18, the radiation pattern in the plane of the antenna ($\phi = 0^{\circ}$) and in the plane perpendicular to the antenna ($\theta = 90^{\circ}$), respectively, are calculated numerically using the CST electromagnetic simulator at different frequencies within the operating band. It can be seen from Fig. 17 that the antenna has almost circular symmetric pattern in the plane normal to the antenna ($\theta = 90^{\circ}$), and omnidirectional with nulls in the z-direction.

For experimental verification of the far-field patterns, a radiation pattern measurement setup is established for this purpose. Some reference-gain horn antennas are used for gain measurement of the entire frequency band of operation ($2.3 - 23$ GHz). During measurement, the reference antenna is maintained oriented to the antenna under test (AUT) which is placed on the rotator for complete rotation in the azimuth and elevation planes. The reference antenna is connected to port 1 of the VNA whereas the AUT is connected to port 2. While rotating the AUT in the desired plane, the readings of the transmission scattering parameter S_{21} are uniformly acquired over the band of frequencies ($2.3 - 23$ GHz) with the preset resolution. A Matlab® program on the laptop plays the role of a central controller and data processor. It controls the rotation of the AUT and the data acquisition of the VNA and stores the S_{21} data during measurement. When the antenna rotation is completed, the stored S_{21} data is processed, the gain is calculated and the radiation patterns at all the frequencies can be drawn. For example, the measured radiation patterns in the plane $\phi = 90°$ and in the plane $\theta = 90°$ at 12 GHz are presented in Figures 19 and 20 and compared to the radiation patterns obtained by simulation showing good agreement. It is clear that the experimental measurements and the simulation results show good agreement.

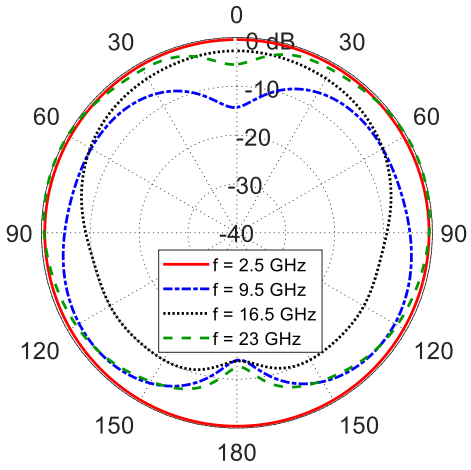

FIGURE 17: Simulated far-field pattern of the SWB antenna in the plane $\phi = 0^{\circ}$.

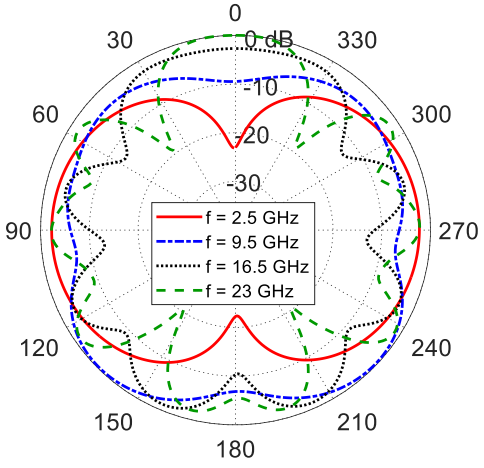

FIGURE 18: Simulated far-field pattern of the SWB antenna in the plane $\theta = 90^{\circ}$.

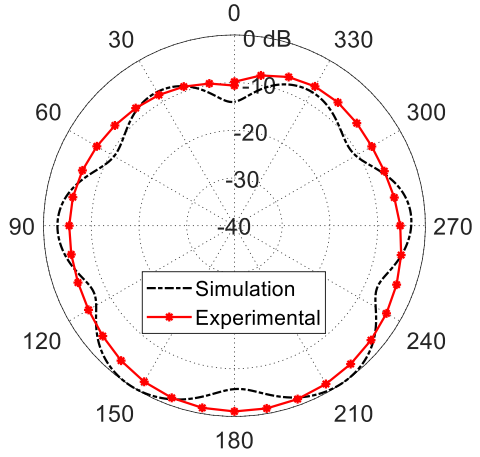

FIGURE 19: Radiation pattern obtained by simulation and measurement for the proposed antenna, at the central frequency (12 GHz) in the plane $\theta = 90^{\circ}$.

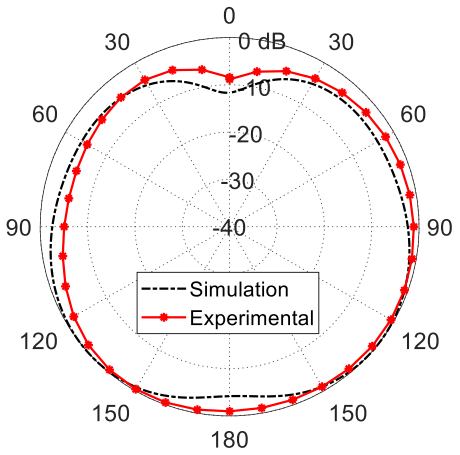

FIGURE 20: Radiation pattern obtained by simulation and measurement for the proposed antenna, at the central frequency (12 GHz) in the plane $\phi = 0^{\circ}$.

F. GAIN AND RADIATION EFFICIENCY OF THE PROPOSED ANTENNA

The gain and radiation efficiency of the proposed antenna are investigated by both electromagnetic simulation and experimental measurement over the frequency band (2.3 – 23 GH). Figure 21 presents the variation of the maximum gain with the frequency over the entire frequency band. The dependence of the radiation efficiency on the frequency is presented in Figure 22. It is shown that the antenna has excellent radiation efficiency over the complete frequency band. For the whole frequency range (2.3 – 23 GHz), the radiation efficiency is higher than 96%. The measured gain and radiation efficiency are compared to the corresponding simulation results showing good agreement.

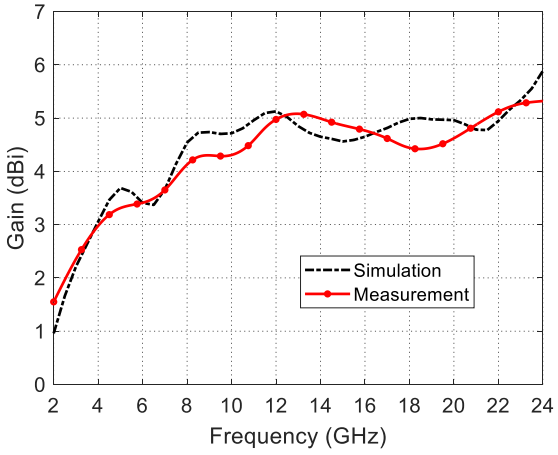

FIGURE 21: Simulated and measured maximum gain with frequency of the SWB antenna shown in Fig. 1.

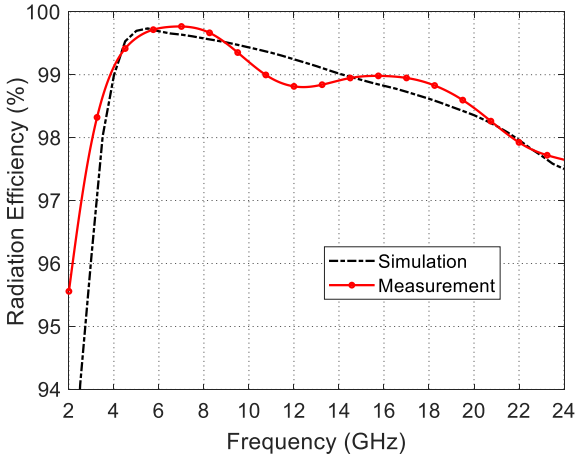

FIGURE 22: Simulated and measured radiation efficiency with frequency of the SWB antenna shown in Fig. 1.

IV. COMPARISON WITH OTHER PUBLISHED WORK

The proposed antenna is compared with similar antennas in other published papers regarding the dimensions, operating bandwidth, bandwidth ratio (BW), bandwidth dimension ratio (BDR), and the antenna efficiency. The comparison table is given in Table 2.

Table 2: comparison of the proposed SWB antenna with similar work

Work	Dimensions (mm × mm)	Frequency Range (GHz)	% BW	RBW	BDR	Radiation Efficiency at Start – End Frequencies
[3]	25.0 × 20.0	3.04 – 17.39	140.6%	5.7: 1	2812	50 – 73%
[7]	35.0 × 30.0	2.8 – 40	173%	14: 1	1647	60 – 70%
[14]	28.0 × 19.0	0.7 – 18.5	185%	26: 1	3400	70 – 80%
[15]	35.0 × 35.0	2.3 – 34.8	175%	15: 1	2403	96 – 52%
[13]	35.0 × 30.0	2.8 – 40	173%	14:1	1904	80 – 82%
[12]	31 × 45	2.1 – 44.5	181%	20:1	3020	95 – 96%
[Present]	56 × 21.2	2.3 – 3.0	164%	10: 1	1360	98 – 96%

V. CONCLUSION

A novel super wide band antenna of more than 96% radiation efficiency is proposed in the present paper. The antenna is composed of diamond-shape two-arm elements printed on the opposite faces of a three-layer dielectric substrate. Each of the antenna arms are reactively coupled to a conducting parasitic element through a narrow gap for enhancing the bandwidth of the antenna. The material of the top and bottom layers of the substrate is Rogers RO3003TM of thickness 0.13 mm, whereas the central layer has dielectric constant of 2.3 and 0.27 mm thickness. The antenna is fabricated and the measurements show good agreement with the results obtained by the CST® simulator. The antenna bandwidth is 20.7 GHz and ranges from 2.3 to 23 GHz. The antenna has a bandwidth to dimension ratio (BDR) of 1360 and minimum radiation efficiency of 96%.

REFERENCES

[1] D. Sagne, and R. A. Pandhare, "Design and Analysis of Inscribed Fractal Super Wideband Antenna for Microwave Applications," Progress In Electromagnetics Research C, Vol. 121, pp. 49-63, 2022.
[2] T. Ali, B. K. Subhash, S. Pathan, and R. C. Biradar, "A compact decagonal-shaped UWB monopole planar antenna with truncated ground plane," Microwave and Optical Technology Letters, Vol. 60, No. 12, pp. 2937–2944, 2018.
[3] R. Azim, M. T. Islam, H. Arshad, M. M. Alam, N. Sobahi, and A. I. Khan, "CPW-fed super-wideband antenna with modified vertical bowtie-shaped patch for wireless sensor networks," IEEEACCESS, Vol. 9, pp. 5343-5353, 2020.
[4] S. Alluri, and N. Rangaswamy, "Compact high bandwidth dimension ratio steering-shaped super wideband antenna for future wireless communication applications," Microwave and Optical Technology Letters, Vol. 62, No. 12, 3985–3991, 2020.
[5] S. Dey, and N. C. Karmakar, "Design of novel super wide band antenna close to the fundamental dimension limit theory," Scientific Reports, Vol. 10, No. 1, 16306, 2020.
[6] M. A. Jamlos, M. F. Jamlos, S. Khatun, and A. H. Ismail, "A compact super wide band antenna with high gain for medical applications," In 2014 IEEE Symposium on Wireless Technology and Applications (ISWTA), pp. 106-109. IEEE, 2014.
[7] S. Kundu, and A. Chatterjee, "A compact super wideband antenna with stable and improved radiation using super wideband frequency selective surface," AEU-International Journal of Electronics and Communications, Vol. 150, No. 154200, 2022.
[8] W. Balani, M. Sarvagya, A. Samasgikar, T. Ali, and P. Kumar, "Design and analysis of super wideband antenna for microwave applications," Sensors, vol. 21, no. 2, No. 477, 2021.
[9] M. A. Dorostkar, M. T. Islam, and R. Azim, "Design of a novel super wide band circular-hexagonal fractal antenna," Progress In Electromagnetics Research 139, 229-245, 2013.
[10] T. Okan, "A compact octagonal-ring monopole antenna for super wideband applications", Microwave and Optical Technology Letters, vol. 62, no. 3, pp. 1237-1244, 2020.
[11] C. K. Ren, C. Sim, R. J. Sheen, "A compact monopole antenna for super wideband applications," IEEE Antennas Wireless and Propagation Letters, vol.10, pp. 488–491, 2011.
[12] M. A. Dorostkar, M. T. Islam, R. Azim, "Design of a novel super wide band circular-hexagonal fractal antenna,", Progress in Electromagnetics Research, vol. 139, pp. 229–245, 2013.
[13] S. Kundu, and A. Chatterjee, "A compact super wideband antenna with stable and improved radiation using super wideband frequency selective surface," AEU-International Journal of Electronics and Communications, vol. 150 No. 154200, 2022.
[14] P. Ramanujam, P. G. R. Venkatesan, C. Arumugam, and M. Ponnusamy, "Design of miniaturized super wideband printed monopole antenna operating from 0.7 to 18.5 GHz," AEU-International Journal of Electronics and Communications 123, 153273, 2020.
[15] S. Alluri and N. Rangaswamy, "Compact high bandwidth dimension ratio steering-shaped super wideband antenna for future wireless communication applications," Microwave and Optical Technology Letters, Vol. 62, no. 12, pp. 3985-3991, 2020.